Progress In Electromagnetics Research, Vol. 125, 219–235, 2012

ENHANCEMENT OF NEAR-INFRARED PHOTONIC BAND GAP IN A DOPED SEMICONDUCTOR PHOTONIC CRYSTAL

H.-C. Hung[1], C.-J. Wu[2,*], T.-J. Yang[3], and S.-J. Chang[1]

[1]Institute of Microelectronics and Department of Electrical Engineering, Center for Micro/Nano Science and Technology, and Advanced Optoelectronic Technology Center, National Cheng Kung University, Tainan 701, Taiwan, R.O.C.

[2]Institute of Electro-Optical Science and Technology, National Taiwan Normal University, Taipei 116, Taiwan, R.O.C.

[3]Department of Electrical Engineering, Chunghua University, Hsinchu 300, Taiwan, R.O.C.

Abstract—In this work, the enhancement in photonic band gap (PBG) in a dielectric-semiconductor photonic crystal (DS PC) is investigated. We consider two possible schemes that can be used to enhance the PBG in the near-infrared region. The first scheme is to add an ultrathin metal layer into the DS PC such that a structure of ternary metal-dielectric-semiconductor (MDS) PC is formed. The second scheme is to make use of the heterostructured PC. In scheme 1, it is found that the addition of metal layer will significantly move the left band edge to the shorter wavelength position, leading to an enlargement in the PBG. This enlargement can be extended as the thickness of metal film is increased. In addition, a pronounced enhancement in PBG is achieved when the metal with a higher plasma frequency is used. In scheme 2, we find that the PBG can be significantly enlarged compared to scheme 1. In addition, the increase in the band extension is shown to be four times larger than that in scheme 1. The results illustrate that, in order to enhance the PBG, the use of scheme 2 is superior to scheme 1. The enhancement of near-infrared (NIR) PBG is of technical use in the optical communications.

Received 3 January 2012, Accepted 22 February 2012, Scheduled 28 February 2012

* Corresponding author: Chien-Jang Wu (jasperwu@ntnu.edu.tw).

1. INTRODUCTION

Photonic crystals (PCs), artificially periodic media, have attracted much attention over the past two decades [1–4]. Depending on the structural dimensions, PCs can be one-, two-, or three-dimensional. The fundamental optical physics, such as the existence of the photonic band gap (PBG), can simply be understood in the one-dimensional (1D) PCs. Simple all-dielectric 1D PCs, which are made of two alternating materials with distinct refractive indices, are also called distributed Bragg reflectors (DBRs) [4]. A DBR functioning as a mirror plays an important part in modern photonics because of its wide use in solid-state lasers.

In practical applications, a PC with wide PBG could be of interest to the community. In optical communications and telecommunications, potentially useful PCs are made of dielectric and semiconducting materials. For instance, a usual binary PC consists of Si and SiO_2 in each period. Such semiconductor-dielectric (SD) PCs can exhibit PBGs in the NIR to mid-IR frequency regions. It is well known that, in the visible region, the bandwidth of PBG in an SDPC like Si/SiO_2 have relatively larger refractive index contrast ($\sim$ 3.46 for Si and 1.46 for SiO_2) than most all-dielectric PCs and thus has a wider PBG, However, in the NIR region, PBG will be reduced because the refractive index of SiO_2 has been increased to 2.25, leading to a decrease in the refractive index contrast [5–7].

To enhance the bandwidth of PBG in a PC, several methods have been proposed thus far. In a binary all-dielectric PC, the PBG can be enlarged by simply increasing the refractive index contrast of the constituents [8]. PBG can also be enhanced in a disordered or chirped PC [9–13]. Using the heterostructured PC, a strongly extended PBG is obtainable [14]. Recently, another scheme of extending PBG is reported, that is, a ternary PC which has three different materials in each period. Optical properties in ternary PCs with different constituent materials have been available [15–19]. Most of them are primarily paid attention to the enhancement of omnidirectional band gaps (OBGs). In [20], Dai et al. use the superconductor in a ternary PC and show that OBG can be markedly extended and be further temperature-tunable because of the temperature-dependent London penetration length in superconductors. Recently, Kong, et al., reported the enhancement in OBG in a one-dimensional ternary plasma PC [21].

Motivated by the ideas of ternary PC together with heterostructured PC, in this work, we would like to analyze the band gap extension for a semiconductor PC in the near-infrared. Two schemes will be proposed to enhance the band gap. In scheme 1, a thin metal layer is

added in the original binary DS PC such that the structure become ternary, i.e., each period is made of metal, dielectric, and semiconductor. The structure of ternary PC is called the MDS PC and is depicted in Figure 1. Here, the semiconductor will be taken to an extrinsic semiconductor, n-Si whose permittivity can be tuned by the impurity concentration. In addition to the band gap extension, this selection also allows us to investigate how the PBG is affected by the doping impurity concentration [22]. The second scheme is to use the photonic heterostructure, i.e., a heterostructured PC is formed by cascading two or more binary DS PCs with different constituent thicknesses in each PC. We will demonstrate that the enhancement of PBG in scheme 2 is superior to that of scheme 1.

The format of paper is given as follows: Section 1 is the introduction. The theoretical method and related materials electromagentics to be used in our calculation are described in Section 2. The numerical results, including the binary and ternary PCs (scheme 1), and the heterostructured PC (scheme 2) are presented in Section 3. The conclusion is then summarized in Section 4.

2. BASIC EQUATIONS

As mentioned in Introduction, we shall use two schemes to enhance the band gap of a DS PC. The structure of the first scheme is shown in Figure 1, in which a structure of one-dimensional ternary metal-

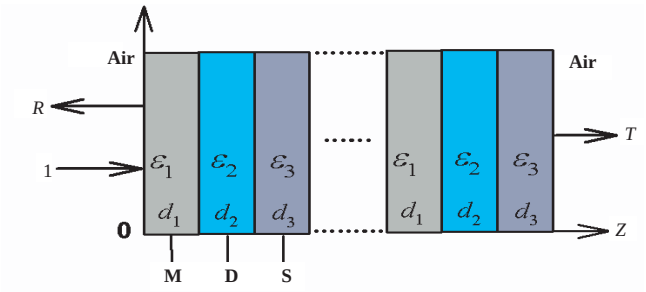

Figure 1. The structure of a one-dimensional ternary metal-dielectric-semiconductor photonic crystal (MDS PC) immersed in air, where, in each period, dielectric layer D is sandwiched by metallic layer M and semiconductor layer S. Here, d_1, d_2, and d_3 are the corresponding thicknesses for layers M, D, and S, respectively. The optical wave with a unit power impinges normally at the plane boundary, $z = 0$. Here, R and T are reflectance and transmittance, respectively.

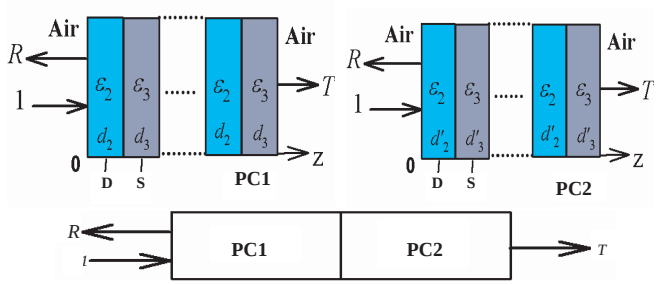

Figure 2. Two binary DS PCs with different thicknesses. The thicknesses of PC2 are denoted as $d'_i = d_i\,(1+\eta)$, $i = 2,\ 3$ and $\eta > 0$. The heterostructured PC is a combination of PC1 and PC2 in series.

dielectric-semiconductor photonic crystal (MDS PC) that is immersed in air. Here, the total number of periods is taken to N_p and the spatial periodicity is $\Lambda = d_1 + d_2 + d_3$, where the thicknesses of the constituent layers are d_1, d_2, and d_3, respectively. In addition, ε_1, ε_2, and ε_3 are the corresponding relative permittivities, respectively. The second scheme, which is depicted in Figure 2, is a combination of two binary PCs in series. The two PCs have different thicknesses in the constituent layers and they are related by

$$d'_i = d_i\,(1+\eta)\,, \qquad i = 2, 3 \text{ and } \eta > 0, \tag{1}$$

where η is regarded as an incremental factor or chirp parameter. Equation (1) illustrates that the constituents' thicknesses of PC2 are taken to be slightly larger than those of PC1.

In scheme 1, the metal layer is added in a DS PC. Thus, it is necessary to describe the permittivity of metals. In what follows, we assume that the temporal part, for all fields, is $\exp(j\omega t)$. With this convention of time part, on the basis of the Drude model, the permittivity of metal layer M is expressed as

$$\varepsilon_1(\lambda) = 1 - \frac{\omega_p^2}{\left(\frac{2\pi c}{\lambda}\right)^2 - j\gamma\frac{2\pi c}{\lambda}}, \tag{2}$$

where ω_p is the plasma frequency and γ is the damping frequency. The index of refraction of M is thus given by $n_1(\lambda) = \sqrt{\varepsilon_1(\lambda)}$. For the semiconductor layer S, we shall consider the extrinsic semiconductor, the n-type silicon (n-Si). For n-Si, its relative permittivity is a function of wavelength and the doping concentration and can be simply expressed in terms of the plasma model, namely [5]

$$\varepsilon_3(\lambda, N) = \varepsilon_\infty\left(1 - \frac{\omega_{pe}^2}{\left(\frac{2\pi c}{\lambda}\right)^2 - j\gamma_e\frac{2\pi c}{\lambda}} - \frac{\omega_{ph}^2}{\left(\frac{2\pi c}{\lambda}\right)^2 - j\gamma_h\frac{2\pi c}{\lambda}}\right), \tag{3}$$

where ε_∞ is the high-frequency limit of the relative permittivity and equal to the permittivity of the intrinsic Si, γ_e and γ_h are the damping frequencies for the electrons and holes, respectively, and ω_{pe}, ω_{ph} are the electron and hole plasma frequencies given by

$$\omega_{pe,\,h} = \sqrt{\frac{n_{e,\,h}e^2}{m_{e,\,h}\varepsilon_0\varepsilon_\infty}}. \tag{4}$$

Here, $m_{e,\,h}$ are the effective masses of electron and hole, $n_{e,\,h}$ are the carrier concentration of electron and hole, respectively. The concentrations of electron and hole are written as [6]

$$n_{e,\,h} = \sqrt{n_i^2 + \frac{N^2}{4}} \pm \frac{N}{2}, \tag{5}$$

where n_i is the intrinsic electron concentration of Si and N is the doping impurity concentration. The corresponding refractive index is then given by

$$n_3(\lambda, N) = \sqrt{\varepsilon_3(\lambda, N)}. \tag{6}$$

The photonic band gap of the PC in scheme 1 of Figure 1 can be investigated by way of the reflectance spectrum. We use the transfer matrix method (TMM) to calculate the reflectance spectrum. According to TMM, we must first compute the total system matrix which can be written as [8]

$$\begin{aligned}\mathbf{M} &= \begin{pmatrix} M_{11} & M_{12} \\ M_{21} & M_{22} \end{pmatrix} \\ &= D_A^{-1}\left(D_1P_1D_1^{-1}D_2P_2D_2^{-1}D_3P_3D_3^{-1}\right)^{N_p}D_A.\end{aligned} \tag{7}$$

where the dynamical matrix D_q ($q = A, 1, 2, 3$), under normal incidence, is expressed as

$$D_q = \begin{pmatrix} 1 & 1 \\ n_q & -n_q \end{pmatrix}, \tag{8}$$

where $q = A$ is for air with $\varepsilon_A = 1$, and N_p is the number of periods. The propagation matrix P_i in Equation (7) for layer i ($i = 1, 2, 3$) takes the form

$$P_i = \begin{pmatrix} \exp(jk_id_i) & 0 \\ 0 & \exp(-jk_id_i) \end{pmatrix}, \tag{9}$$

where $k_i = n_i(2\pi/\lambda)$ is the associated wave number. The reflectance R and transmittance T are then given by

$$R = \left|\frac{M_{21}}{M_{11}}\right|^2, \quad T = \left|\frac{1}{M_{11}}\right|^2. \tag{10}$$

The absorptance is $A = 1 - R - T$.

The PBG structure in a PC can also be investigated by directly plotting the dispersion relation K vs λ, where K is the Bloch wave number. To compute the dispersion relation, we have to determine the translation matrix for a single period, M_s, which is expressible as

$$\mathbf{M_s} = \begin{pmatrix} A & B \\ C & D \end{pmatrix} = D_1^{-1} D_2 P_2 D_2^{-1} D_3 P_3 D_3^{-1} D_1 P_1. \tag{11}$$

This matrix relates the complex amplitudes of the incident wave a_{n-1} and the reflected wave b_{n-1} in one layer of a period to those of the same layer in the next period, i.e.,

$$\begin{pmatrix} a_{n-1} \\ b_{n-1} \end{pmatrix} = \begin{pmatrix} A & B \\ C & D \end{pmatrix} \begin{pmatrix} a_n \\ b_n \end{pmatrix}. \tag{12}$$

According to the Bloch theorem, field solution can be expressed as a Bloch form, namely

$$E_K(z,t) = E_K(z)\, e^{-jKz} e^{j\omega t}, \tag{13}$$

where K is the Bloch wave vector, and the amplitude is a periodic function of spatial periodicity, i.e., $E_K(z+\Lambda) = E_K(z)$. Then the dispersion relation can be determined by the following relation, i.e.,

$$\cos(K\Lambda) = \frac{1}{2}(A + D). \tag{14}$$

An explicit expression for Equation (14) can be obtained as [16]

$$\cos(K\Lambda) = \cos\beta_1 \cos\beta_2 \cos\beta_3 - \frac{1}{2}\left(\frac{n_1}{n_2} + \frac{n_2}{n_1}\right) \sin\beta_1 \sin\beta_2 \cos\beta_3$$
$$-\frac{1}{2}\left(\frac{n_2}{n_3} + \frac{n_3}{n_2}\right) \cos\beta_1 \sin\beta_2 \sin\beta_3 - \frac{1}{2}\left(\frac{n_1}{n_3} + \frac{n_3}{n_1}\right) \sin\beta_1 \cos\beta_2 \sin\beta_3, \tag{15}$$

where $\beta_\ell = k_0 n_\ell d_\ell$, $\ell = 1$, 2, and 3, with $k_0 = \omega\sqrt{\mu_0 \varepsilon_0}$ being the free-space wave number. For a binary PC, say $d_3 = 0$, Equation (15) reduces to [8]

$$\cos(K\Lambda) = \cos\beta_1 \cos\beta_2 - \frac{1}{2}\left(\frac{n_1}{n_2} + \frac{n_2}{n_1}\right) \sin\beta_1 \sin\beta_2. \tag{16}$$

In general, the Bloch wave number is complex-valued, $K = K_r - jK_i$. In the PBGs (stop bands), solution for K has an imaginary part K_i so that the Bloch wave is evanescent. In the transmission band, where the Bloch wave is a propagation mode because the solution for K is purely real, i.e., $K = K_r$. It should be noted that, in the presence of loss, A and D in Equation (11) are with imaginary parts which, in turn, have a salient effect on Equations (14)–(16), that is, we will have a

so-called complex photonic band structure (CPBS). In this case, Bloch wave number K (and $\cos(K\Lambda)$) will be complex everywhere (not only in the PBG but also in the transmission band) [23].

As for the scheme 2 of Figure 2, the PBG extension will be investigated on the basis of the calculated reflectance using TMM. In this case, the total system matrix of a heterostructured PC is written as

$$\begin{aligned}\mathbf{M} &= \begin{pmatrix} M_{11} & M_{12} \\ M_{21} & M_{22} \end{pmatrix} \\ &= D_A^{-1}\left(D_2 P_2 D_2^{-1} D_3 P_3 D_3^{-1}\right)^{N_p}\left(D_{2'} P_{2'} D_{2'}^{-1} D_{3'} P_{3'} D_{3'}^{-1}\right)^{N_p} D_A. \quad (17)\end{aligned}$$

The reflectance can be calculated from Equation (10).

Before presenting the numerical results, let us discuss the loss factor arisen from the n-Si. In our calculation the doping concentration will be taken on the order of $10^{19}\,\mathrm{cm}^{-3}$ in n-Si. In this case, the strongly doped semiconductor has absorption coefficient α on the order of $100\,\mathrm{cm}^{-1}$ [24]. Because α will be directly related to γ_e and γ_h in Equation (3), the damping frequencies for the electrons and holes, respectively, it is thus necessary to establish the relationship of how to get γ_e and γ_h from α. Since we are interested in the strongly doped n-Si, the third term in the bracket (contributed by holes) is negligibly small and can be reasonably omitted. Thus, the permittivity in Equation (3) becomes

$$\begin{aligned}\varepsilon_3(\lambda, N) &= \varepsilon_3' - j\varepsilon_3'' \\ &= \varepsilon_\infty\left(1 - \frac{\omega_{pe}^2}{\left(\frac{2\pi c}{\lambda}\right)^2 - j\gamma_e\frac{2\pi c}{\lambda}}\right) = \varepsilon_\infty\left(1 - \frac{\omega_{pe}^2}{\omega^2 - j\gamma_e\omega}\right). \quad (18)\end{aligned}$$

The wavenumber of n-Si can be written by

$$k_3 = \frac{2\pi}{\lambda}\, n_3 = \frac{2\pi}{\lambda}\left(\bar{n}_3 - j\bar{k}_3\right) = \frac{2\pi}{\lambda}\sqrt{\varepsilon_3' - j\varepsilon_3''}, \quad (19)$$

where the imaginary part $\bar{k}_3$ is directly related to the absorption coefficient α, namely [8]

$$\alpha = \frac{4\pi}{\lambda}\bar{k}_3. \quad (20)$$

With Equation (19), a direct manipulation leads to

$$\alpha = \frac{4\pi}{\lambda}\frac{1}{\sqrt{2}}\left[\sqrt{\sqrt{\varepsilon_3'^2 + \varepsilon_3''^2} - \varepsilon_3'}\right], \quad (21)$$

where ε_3' and ε_3'' are obtainable from Equation (18), with the results

$$\varepsilon_3' = \varepsilon_\infty\left(1 - \frac{\omega_{pe}^2}{\omega^2 + \gamma_e^2}\right); \quad \varepsilon_3'' = \varepsilon_\infty\frac{\gamma_e\omega_{pe}^2}{\omega^3 + \gamma_e^2\omega}. \quad (22)$$

Equations (21) and (22) enable us to numerically determine γ_e when α is given.

3. NUMERICAL RESULTS AND DISCUSSION

3.1. Enhancement of Band Gap Structure by a Metal Film

In the next calculation, we shall focus on the PBG structure in the NIR region, in fact, 1–2 μm. The metallic layer M is taken to be silver (Ag) with plasma frequency $\omega_p = 2\pi \times 2.175 \times 10^{15}$ rad/s and damping frequency $\gamma = 2\pi \times 4.35 \times 10^{12}$ rad/s [25]. The dielectric layer D is SiO_2 with $n_2 = 2.25$ [7]. The semiconductor layer S is taken to be n-Si with $\varepsilon_\infty = 11.7$ [6]. By taking $\alpha = 100\,\text{cm}^{-1}$, the average value of electron damping frequency can be found to be $\gamma_e = 9.375$, 47.385, 94.801, and 189.617 rad/s for $N = 1 \times 10^{19}$, 5×10^{19}, 10×10^{19}, and $20 \times 10^{19}\,\text{cm}^{-3}$ according to Equations (21) and (22), where $\lambda = 1.5\,\mu\text{m}$ is fixed. These values in γ_e together with $\gamma_h = 0$ will be adopted in the following calculation.

In Figure 3, we plot the PBGs for both the binary DS PC (black curve) and the ternary MDS PC (red curve). Here, the thicknesses

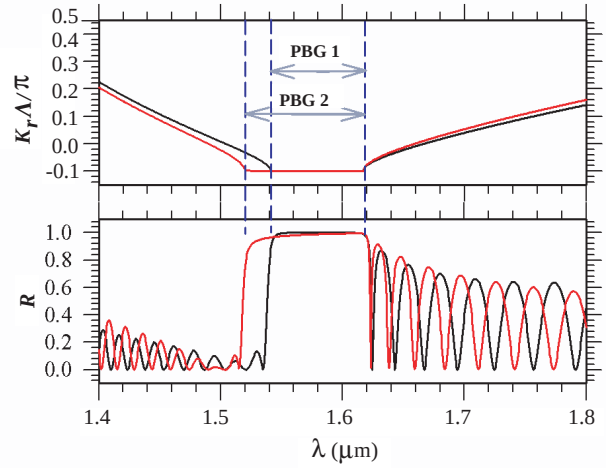

Figure 3. The calculated PBGs for the binary DS PC (without M) and ternary MDS PC. The black curve is for the binary PC with $d_2 = 0.8$ and $d_3 = 0.4\,\mu\text{m}$ whereas the red curve is for ternary PC with an additional metal layer of $d_1 = 1\,\text{nm}$. In calculating R, the number of periods, $N_p = 15$, is taken for both PCs.

of layers D and S are $d_2 = 0.8$ and $d_3 = 0.4\,\mu\text{m}$. In ternary PC, the metallic layer M has a thickness of $d_1 = 1\,\text{nm}$. The impurity concentration in n-Si is $N = 1 \times 10^{19}\,\text{cm}^{-3}$. It can be seen from Figure 3 that the PBG 1 of binary PC has been enhanced to PBG 2 when the metallic layer is added. The PBG in the original binary PC is $\sim 0.08\,\mu\text{m}$. The right band edges of both PCs nearly coincide, but the left band edge of ternary PC moves to a shorter wavelength. As a result, the PBG is enhanced due to the presence of metal layer. In ternary PC, the high reflectance range (HRR), in R-curve, is not so flat as in binary PC, especially in the region close to the left band edge. This slight deviation can be ascribed to the fact that we have incorporated loss factor γ in Ag.

Keeping the same material parameters in Figure 3, Figure 4 depicts the PBG structures for the ternary PC at different thicknesses of layer M. Here, the upper panel is the photonic band structure for the infinite PC structure. The corresponding reflectance for a finite PC structure (15 periods) is demonstrated in the lower panel. Good consistence is obtained for both two plots. The PBG can be enlarged by increasing the thickness of the metal layer. It is seen that there exists a PBG in the vicinity of wavelength $1.5\,\mu\text{m}$ with different thicknesses of metal layer. The left band edge has been significantly moved to the shorter wavelength as the metal thickness increases. The shift in the right band edge is not so pronounced as the left one. In addition, the left band edge in the reflectance spectrum becomes sharper and flat when the thickness of metal layer is increased. With the salient shift in the left band edge, the PBG is thus enlarged considerably at a thicker metallic layer. The other effect in the thick metal is that the magnitudes of the reflectance in the pass bands have been increased significantly, causing to weaken the wave transmission through the PC. The role played by thin metal layer in the ternary PC is thus elucidated.

In Figure 4, we have fixed the number of periods of the PC. Since the loss factor is incorporated, we continue to investigate the thickness effect in the reflectance spectrum by changing the number of periods. The result is depicted in Figure 5, where the thickness of metal is fixed at $d_1 = 10\,\text{nm}$. It can be seen that although the metallic loss included, the PBG does not substantially affected by the number of periods. The effect is salient only in the pass bands, the Fabry-Perot-like oscillations.

We now investigate how the PBG is enhanced with different metal layer. In Figure 6, we plot the PBGs in a ternary PC for different metal layer, Cu, Ag, and Al. The calculated conditions are $d_1 = 5\,\text{nm}$, $d_2 = 0.8$, $d_3 = 0.4\,\mu\text{m}$, and $N = 1 \times 10^{19}\,\text{cm}^{-3}$. The plasma and damping frequencies for Cu, Ag, and Al are $\omega_p = 2\pi \times 1.914 \times 10^{15}$, $2\pi \times 2.175 \times 10^{15}$, $2\pi \times 3.570 \times 10^{15}\,\text{rad/s}$, and $\gamma = 2\pi \times 8.34 \times 10^{12}$,

$2\pi \times 4.35 \times 10^{12}$, $2\pi \times 19.4 \times 10^{12}$ rad/s, respectively [25]. It can be seen that the PBG enhancement is pronounced for Al, which has the largest plasma frequency among them. The inclusion of damping frequency leads to smoothing the left band edge, especially for Al. The smooth in the left band (shorter wavelength) reflects the presence of complex photonic band structure if the loss is considered. Another feature is of note, i.e., using Al, the oscillations in the pass bands become nearly unseen, as pictured in the reflectance plot. Based on the results of Figures 4 and 6, we conclude that, in order to have a wide PBG, it is better to select a metal with higher plasma frequency and thicker film.

As we have known that permittivity of n-Si is dependent on the

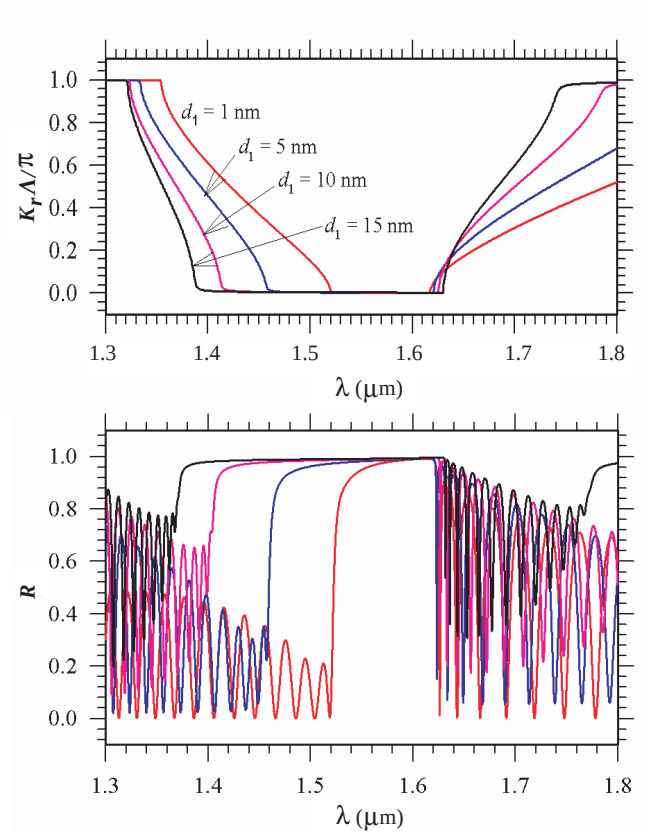

Figure 4. The calculated PBGs for a ternary MDS PC at $d_2 = 0.8$ and $d_3 = 0.4\,\mu$m at different thicknesses of metal layer, $d_1 = 1$ (red), 5 (blue), 10 (pink), and 15 (black) nm, respectively. The enlargement in PBG is obvious at a larger d_1. The reflectance spectrum for a finite MDS PC with 15-period is shown in the lower panel.

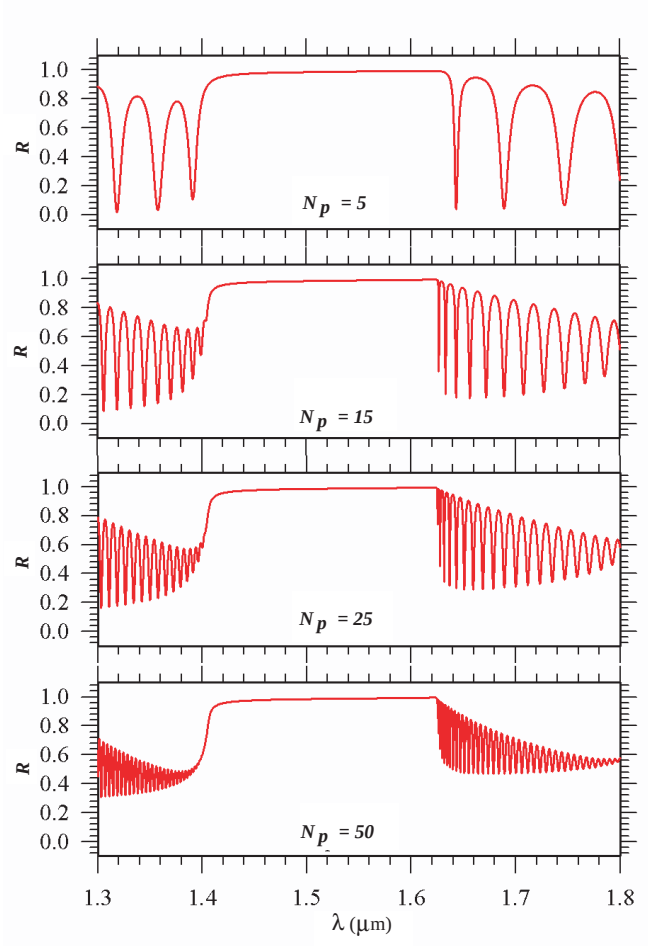

Figure 5. The calculated PBGs for a ternary MDS PC at $d_2 = 0.8$, $d_3 = 0.4\,\mu$m, and $d_1 = 10\,$nm for different numbers of periods, $N_p = 5$, 15, 25, and 50, respectively.

impurity concentration, it is thus worthy of examining the dependence of PBG on the impurity concentration. With different concentrations, different values in γ_e can be obtained by Equations (21) and (22), as given in Subsection 3.1. The results are plotted in Figure 7, in which the conditions $d_1 = 5\,$nm, $d_2 = 0.8$, $d_3 = 0.4\,\mu$m, and M = Ag, are used. It is seen that the whole PBG of interest is shifted to the left as N increases.

Before going on to the next scheme for the band gap extension, let us discuss how the above numerical results agree with experimental

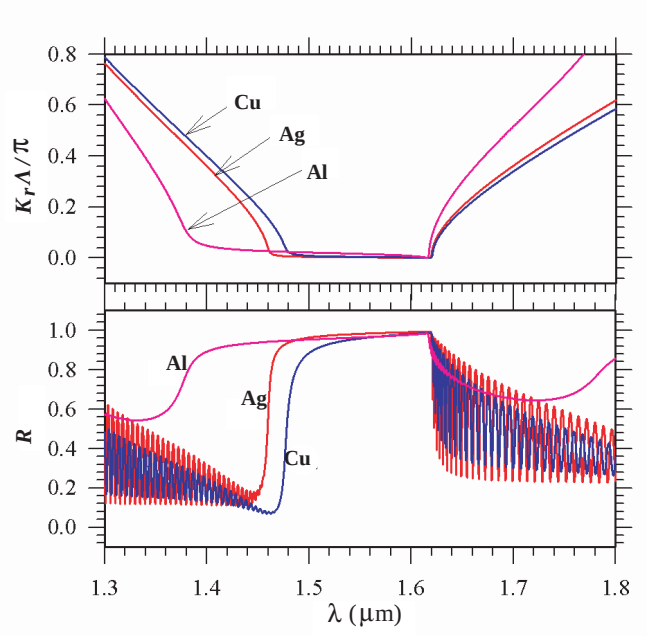

Figure 6. The calculated PBGs for a ternary MDS PC at $d_1 = 5\,\text{nm}$, $d_2 = 0.8$ and $d_3 = 0.4\,\mu\text{m}$ for different metals, Cu (blue), Ag (red), and Al (pink). The reflectance spectra are calculated at $N_p = 50$.

results. As shown in Figure 4, we have seen that the left band edge can be moved to the left, i.e, blue-shifted, such that the PBG can be enlarged. The shift to a shorter wavelength means that the right band edge in the frequency domain is shifted to a higher frequency. Such a shifting behavior has been experimentally reported by Keskinen et al. [26]. In Figure 8 of their work, the authors have measured the transmittance spectrum for an MDPC with M = Ag. The right band edge is apparently shown to be blue-shifted as the thickness of Ag increases, which is consistent with the result given in Figure 4. Thus, the PBG enhancement due to the presence of metal layer in a photonic crystal is clearly elucidated.

3.2. Enhancement of Band Gap Structure by a Heterostructure PC

Let us now investigate the PBG enhancement based on the use of scheme 2 in Figure 2. With the same parameters used in the calculations of Figure 3, in Figure 8, we have plotted the reflectance spectra for PC1, PC2, and PC1+PC2, where the incremental factor

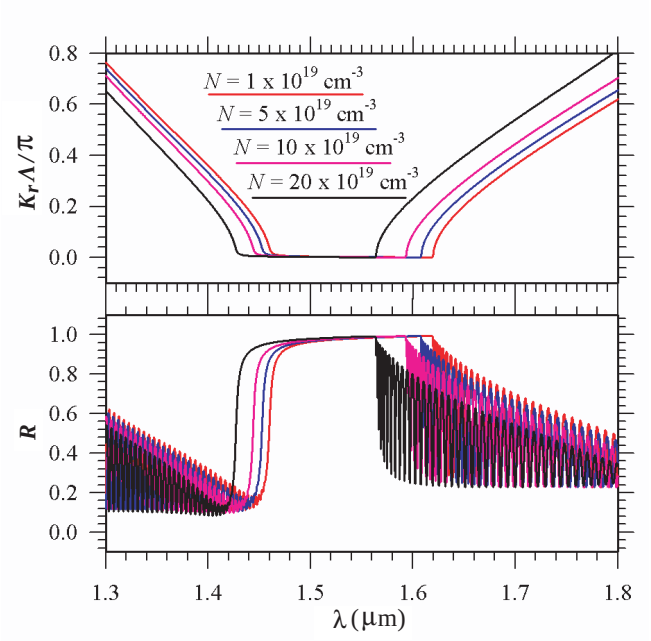

Figure 7. The calculated PBGs for a ternary MDS PC at $d_1 = 5\,\text{nm}$, $d_2 = 0.8$ and $d_3 = 0.4\,\mu\text{m}$ for different impurity concentrations of n-Si, $N = 1\times10^{19}$ (red), 5×10^{19} (blue), 10×10^{19} (pink) and $20\times10^{19}\,\text{cm}^{-3}$ (black).

in Equation (1) is taken to be $\eta = 0.04$. We see that the PBG enhancement in PC1+PC2 is much efficient compared to the scheme 1 in Figure 3. In Figure 3, the addition of thin metal layer increases the gap width by only $\sim 0.02\,\mu\text{m}$. However, in Figure 8, the magnitude in the increase of gap width is about $0.08\,\mu\text{m}$, nearly four times larger than the enhanced scheme 1. The PBG enlargement in the heterostructure PC can occur only when the PBGs of PC1 and PC2 must (partially) overlap each other, as illustrated by two vertical blue dashed lines. The resultant PBG of PC1+PC2 ranges from the left band edge of PC1 to the right band edge of PC2, as shown by the two vertical red dashed lines.

It is worthy to mention that the choice of chirp parameter in Equation (1) is crucial. Increasing η will significantly shift the PBG structure of PC1 to the right. For example, if $\eta = 0.1$ is used, then the shift to the right is too large such that there is no overlapping between two PBGs. As a result, the goal of band gap extension will not be reached.

Following this series combination, it is possible to continue to get

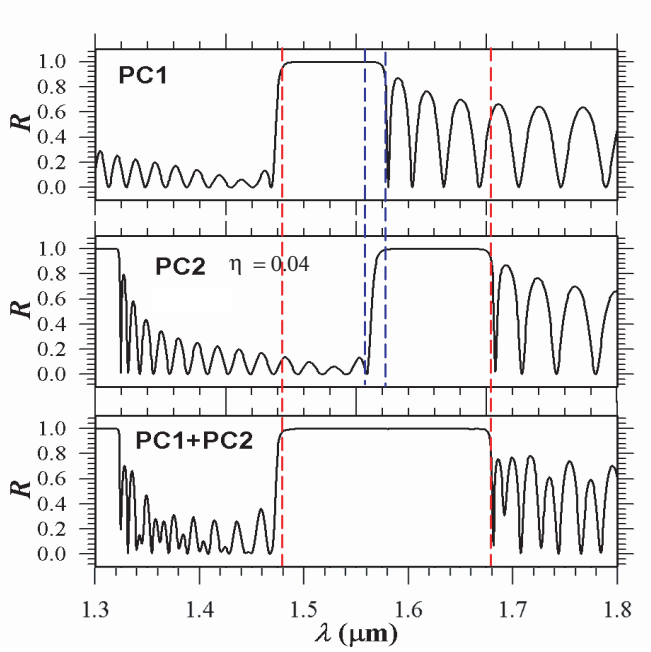

Figure 8. The calculated reflectance spectra for the binary DS PC1 at $d_2 = 0.8$, $d_3 = 0.4\,\mu$m, PC2 at $d_2 = 0.8(1 + 0.04)$, $d_3 = 0.4(1 + 0.04)\,\mu$m, and a series of combination of PC1 and PC2 for impurity concentrations of n-Si, $N = 1 \times 10^{19}\,\mathrm{cm}^{-3}$.

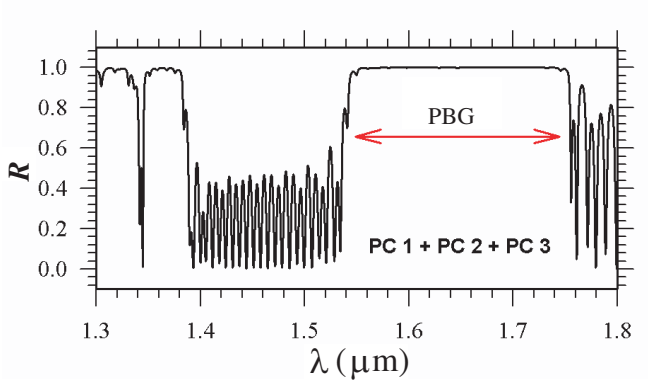

Figure 9. The calculated reflectance spectra for the heterostructured PC of PC1+PC2+PC3. Here in PC1, $d_2 = 0.6$, $d_3 = 0.2\,\mu$m, in PC2, $d_2 = 0.8(1+0.04)$, $d_3 = 0.4(1+0.04)\,\mu$m, and in PC3, $d_2 = 0.8(1+0.08)$, $d_3 = 0.4(1 + 0.08)\,\mu$m.

a wider PBG by cascading three binary PCs, i.e., PC1+PC2+PC3, where PC3 is assigned to have the thicknesses of Equation (1). Taking $\eta = 0.04$ for PC2 and $\eta = 0.08$ for PC3, the band gap extension is demonstrated in Figure 9. It is apparent that the PBG is greatly enhanced compared to that of PC1+PC2 in Figure 8. The right band edge is now extended to near 1.75 μm, leading to a much broader PBG.

4. CONCLUSION

We have studied the photonic band gap extension in a semiconductor-dielectric PC in the near-infrared region. We have examined two possible schemes. One is a ternary MDS PC. The other is the use of photonic heterostructure. In scheme 1, it is found that the PBG can be enlarged when a thin metal layer is incorporated. It can be further enhanced if the thickness of metal layer is increased. Using a metal layer with higher plasma frequency, it is beneficial to get the wider PBG. The change in the impurity concentration in n-Si will cause the PBG structure to be shifted to the shorter wavelength region. However, no substantial extension in PBG due to the variation of concentration is seen. In scheme 2, we find that the enhancement in the PBG is much more efficient compared to scheme 1. It can be used to obtain a much boarder PBG that is of technical use in semiconductor optoelectronics. Finally in our calculations, we have considered all the losses coming from the metal layer as well as the n-Si. Such factors are usually neglected in the previous reports.

ACKNOWLEDGMENT

C.-J. Wu acknowledges the financial support from the National Science Council (NSC) of Taiwan, R.O.C. under Contract No. NSC-100-2112-M-003-005-MY3 and from the National Taiwan Normal University under NTNU100-D-01.

S.-J. Chang would like to thank the NSC and Bureau of Energy, Ministry of Economic Affairs of Taiwan, R.O.C. for the financial support under Contract No. NSC-100-2221-E-006-040-MY2 and 100-D0204-6 and the LED Lighting Research Center of NCKU.

REFERENCES

1. Markos, P. and C. M. Soukoulis, *Wave Propagation: From Electrons to Photonic Crystals and Left-Handed Materials*, Princeton University Press, New Jersey, 2008.

2. Joannopoulos, J. D., R. D. Meade, and J. N. Winn, *Photonic Crystals: Molding the Flow of Light*, Princeton University Press, Princeton, NJ, 1995.
3. Sakoda, K., *Optical Properties of Photonic Crystals*, Springer-Verlag, Berlin, 2001.
4. Orfanidis, S. J., *Electromagnetic Waves and Antennas*, Rutger University, 2008, www.ece.rutgers.edu/ orfanidi/ewa.
5. Sàncheza, A. S. and P. Halevi, "Simulation of tuning of one-dimensional photonic crystals in the presence of free electrons and holes," *J. Appl. Phys.*, Vol. 94, 797–799, 2003.
6. Galindo-Linares, E., P. Halevi, and A. S. Sàncheza, "Tuning of one-dimensional Si/SiO_2 photonic crystals at the wavelength of 1.54 μm," *Solid State Comm.*, Vol. 142, 67–70, 2007.
7. Hung, H.-C., C.-J. Wu, and S.-J. Chang, "Terahertz temperature-dependent defect mode in a semiconductor-dielectric photonic crystal," *J. Appl. Phys.*, Vol. 110, 093110, 2011.
8. Yeh, P., *Optical Waves in Layered Media*, John Wiley & Sons, Singapore, 1991.
9. Wu, C.-J., B.-H. Chu, and M.-T. Weng, "Analysis of optical reflection in a chirped distributed Bragg reflector," *Journal Electromagnetic Waves and Applications*, Vol. 23, No. 1, 129–138, 2009.
10. Li, H., H. Chen, and X. Qiu, "Bandgap extension of disordered 1D binary photonic crystals," *Physica B*, Vol. 279, Nos. 1–3, 164–167, 2000.
11. Tolmachev, V. A., T. S. Perova, J. A. Pilyugina, and R. A. Moore, "Experimental evidence of photonic band gap extension for disordered 1D photonic crystals based on Si," *Optics Comm.*, Vol. 259, No. 1, 104–106, 2006.
12. Qi, L., Z. Yang, X. Gao, F. Lan, Z. Shi, and Z. Liang, "Bandgap extension of disordered one-dimensional metallic-dielectric photonic crystals," *IEEE International Vacuum Electronics Conference*, 158–159, 2008.
13. Wu, C.-J., Y.-N. Rao, and W.-H. Han, "Enhancement of photonic band gap in a disordered quarter-wave dielectric photonic crystal," *Progress In Electromagnetics Research*, Vol. 100, 27–36, 2010.
14. Wang, X., X. Hu, Y. Li, W. Jia, C. Xu, X. Liu, and J. Zi, "Enlargement of omnidirectional total reflection frequency range in one-dimensional photonic crystals by using photonic heterostructures," *Appl. Phys. Lett.*, Vol. 80, No. 23, 4291–4293, 2002.

15. Srivastava, R., S. Pati, and S. P. Ojha, "Enhancement of omnidirectional reflection in photonic crystal heterostructures," *Progress In Electromagnetics Research B*, Vol. 1, 197–208, 2008.
16. Awasthi, S. K., U. Malaviya, and S. P. Ojha, "Enhancement of omnidirectional total-reflection wavelength range by using one-dimensional ternary photonic bandgap material," *J. Opt. Soc. Am. B: Optical Physics*, Vol. 23, 2566–2571, 2006.
17. Banerjee, A., "Enhanced refractometric optical sensing by using one-dimensional ternary photonic crystals," *Progress In Electromagnetics Research*, Vol. 89, 11–22, 2009.
18. Banerjee, A., "Enhanced incidence angle based spectrum tuning by using one-dimensional ternary photonic band gap structures," *Journal of Electromagnetic Waves and Applications*, Vol. 24, 1023–1032, 2010.
19. Wu, C.-J., Y.-H. Chung, B.-J. Syu, and T.-J. Yang, "Band gap extension in a one-dimensional ternary metal-dielectric photonic crystal," *Progress In Electromagnetics Research*, Vol. 102, 81–93, 2010.
20. Dai, X. Y., Y. J. Xiang, and S. C. Wen, "Broad omnidirectional reflector in the one-dimensional ternary photonic crystals containing superconductor," *Progress In Electromagnetics Research*, Vol. 120, 17–34, 2011.
21. Kong, X. K., S.-B. Liu, H.-F. Zhang, C.-Z. Li, and B.-R. Bian, "Omnidirectional photonic band gap of one-dimensional ternary plasma photonic crystals," *J. Optics*, Vol. 13, 035101, 2011.
22. Wu, C.-J., Y.-C. Hsieh, and H.-T. Hsu, "Tunable photonic band gap in a doped semiconductor photonic crystal in near infrared region," *Progress In Electromagnetics Research*, Vol. 114, 271–283, 2011.
23. Morozov, G. V., F. Placido, and D. W. L. Sprung, "Absorptive photonic crystals in 1D," *J. Optics*, Vol. 13, 035102, 2011.
24. See http://www.ioffe.ru/SVA/NSM/Semicond/Si/optic.html.
25. Marquez-Islas, R., B. Flores-Desirena, and F. Pérez-Rodríguez, "Exciton polaritons in one-dimensional metal-semiconductor photonic crystal," *J. Nanosci. Nanotechnol.*, Vol. 8, 6584–6588, 2008.
26. Keskinen, M. J., P. Loschialpo, D. Forester, and J. Schelleng, "Photonic band gap structure and transmissivity of metal-dielectric systems," *J. Appl. Phys.*, Vol. 88, 5785–5790, 2000.